Am J Transl Res 2025;17(12):9830-9845
www.ajtr.org /ISSN:1943-8141/AJTR0169292

Original Article

Sea buckthorn flavonoids attenuate oxidative stress in hepatocellular carcinoma via suppression of PI3K/Akt and JAK pathways

Huimin Zhang[1], Haiying Huang[1], Fuqing Miao[1], Ji Nan[2]

[1]*Department of Food Technique and Engineering, Vocational and Technical College of Inner Mongolia Agricultural University, Baotou 014100, Inner Mongolia, China;* [2]*Medical Innovation Center for Nationalities, Inner Mongolia Medical University, Hohhot 010110, Inner Mongolia, China*

Received October 13, 2025; Accepted December 4, 2025; Epub December 15, 2025; Published December 30, 2025

Abstract: Objective: Sea buckthorn is rich in flavonoid components that possess significant antioxidant capacity, capable of eliminating free radicals, reducing oxidative damage, and demonstrating inhibitory effects on the proliferation of various cancer cell lines. The total flavonoids of sea buckthorn (SFs) and its monomers have shown their effect in inhibiting the proliferation of human liver cancer cells in vitro, accompanied by a decrease in intracellular oxidative stress indicators. Although current research results indicate that SFs have antioxidant and anti-hepatocellular carcinoma activities, there is still a lack of precise molecular mechanism studies on their role in Hepatocellular carcinoma (HCC). Methods: SFs were extracted using an ultrasonication-assisted ammonium sulfate-ethanol method and characterized by LC-MS. Network pharmacology identified core targets, which were subsequently validated through molecular docking and dynamics simulations. In vitro, the antioxidant capacity of SFs was assessed using 2,2-diphenyl-1-picrylhydrazyl (DPPH), 2,2'-azino-bis(3-ethylbenzothiazoline-6-sulfonic acid (ABTS), Peroxyl Radical Scavenging Capacity (PSC), and Total Antioxidant Capacity (TOAC) assays. The effects of SFs on HepG2 cell viability and apoptosis were evaluated using CCK-8 and flow cytometry assays, respectively. Oxidative stress-related factors were measured by ELISA. Western blot and qPCR were used to determine the effect of SFs on the PI3K/Akt and JAK signaling pathways. Result: LC-MS identified 1,988 compounds, including key flavonoids such as chrysin, hesperetin, acacetin, and nobiletin. Network pharmacology highlighted PI3K and JAK as core targets. To reveal the relationship between SFs and core target, molecular docking was used to find binding affinities between these key flavonoids and the core targets, which was corroborated by stable molecular dynamics simulations. Furthermore, we found that SFs exerted their antioxidant, anti-apoptotic, and anti-inflammatory effects through the inhibition of the PI3K/Akt and JAK pathways. Conclusion: This study demonstrates that SFs attenuate oxidative stress in HepG2 cells by scavenging free radicals, inhibiting pro-inflammatory cytokines, and modulating the PI3K/Akt and JAK pathways. These findings position SFs as a strong candidate for further preclinical development as an adjuvant therapy for HCC.

Keywords: Flavonoids from sea buckthorn, oxidative stress, hepatocellular carcinoma, PI3K/Akt, JAK

Introduction

Hepatocellular carcinoma (HCC) is one of the most frequently diagnosed malignant tumors worldwide, with an estimated 906,000 new cases globally in 2020. It is the third most common cause of cancer-related deaths, with a 5-year relative survival rate of approximately 18% [1, 2]. What is even more worrying is that in 2023, the United States saw 41,210 new cases of HCC, an increase of nearly three times over the past 40 years [3]. These patients suffer from HCC for various reasons, such as hepatitis B virus (HBV) infection, alcoholic steatohepatitis (ASH), or non-alcoholic fatty liver disease (NAFLD). These pathogenic factors disrupt the balance between growth-promoting oncogenes and tumor suppressor genes in liver cells, leading to abnormal activation of key signaling pathways [4, 5]. The pathways, including the PI3K/Akt/mTOR, JAK/STAT, Ras/Raf/MAPK, and Wnt/β signaling pathways have been prov-

en to have a strong correlation with the development and progression of HCC, and play fundamental and crucial roles in coordinating important cellular processes such as cell proliferation, cell lineage specialization, programmed cell death, and the response of HCC to oxidative stress. Therefore, they are key therapeutic targets in current anti-cancer drug research and development [6, 7].

The link between oxidative stress and HCC progression is also well-established, making redox homeostasis as a compelling therapeutic target. Elevated reactive oxygen species (ROS) directly drives tumorigenesis by inducing DNA mutagenesis and activating pro-oncogenic signaling pathways, such as the PI3K/Akt pathway. Further, active cancer state is often exacerbated by the enhanced aerobic glycolysis characteristic of malignant cells, which increases ROS production, forming a positive feedback loop [8]. Additionally, HCC models show that oxidative stress can upregulate specific effectors, like HEXB, to accelerate tumor progression [9]. This concept is supported by evidence that various antioxidants, including curcumin, vitamins C and E, and silymarin, can mitigate HCC progression by modulating specific effectors to scavenge ROS and protect against DNA damage in hepatic tissues [10-12].

Sea buckthorn (*Hippophae rhamnoides L.*), a plant distributed across Europe and Asia, is a rich source of bioactive compounds. Its flavonoids, including flavonols, flavanols, and flavanones, are considered the primary active constituents, demonstrating potent antioxidative, antitumor, anti-inflammatory, and lipid-lowering properties [13, 14]. Regarding the antioxidant function of SFs, they can regulate Lectin-like oxidized low-density lipoprotein receptor-1 (LOX-1) and endothelial nitric oxide synthase (eNOS) gene transcription to shield endothelial cells from oxidized low-density lipoprotein injury [15]. Quercetin is a key compound included in SFs, and has been shown to inhibit the proliferation of HepG2 and Huh7 hepatocellular carcinoma cell lines by activating the JAK/STAT pathway and enhancing IFN-α responsive gene transcription [16]. Additionally, other studies show that SFs with neurotrophic properties can enhance neuronal maturation through activation of the PI3K/Akt cascade and ERK-mediated pathways. This effect is likely attributed to polyphenolic compounds including kaempferol, isorhamnetin, and quercetin [17].

Given the antioxidant and anti-tumor properties of SFs, we isolated it using ultrasonication-assisted ammonium sulfate-ethanol extraction, followed by qualitative and quantitative analyses to identify and profile the resulting flavonoid constituents. Network pharmacology identified PI3K and JAK as core SFs targets. Computational analyses, including molecular docking and dynamic simulation approaches, demonstrated that major constituents of SFs form stable complexes and exhibit high affinity interactions with the active sites of PI3K and JAK proteins. In vitro validation demonstrated SF-mediated antioxidant effects, modulation of HepG2 cell viability, apoptotic activity, inflammatory cytokine levels, and suppression of PI3K/Akt and JAK signaling pathways.

Materials and methods

Extraction of flavonoids from seabuckthorn

Sea buckthorn was first pulverized into a fine powder and then subjected to petroleum ether extraction to eliminate fats and some pigments. The defatted powder (1.25 g) was mixed with an ammonium sulfate-ethanol aqueous two-phase system (20 mL, 50% ethanol concentration). The mixture underwent ultrasonic-assisted extraction at 60°C for 40 min using an ultrasonic oscillator, followed by filtration to obtain the flavonoid extract.

Compositional analysis of SFs

The extract was lyophilized for 63 h in freeze dryer (Scientz-100F) and pulverized (30 Hz, 1.5 min) on a mill (MM 400, Retsch) until powdered. A 50 mg portion of the powdered sample was thoroughly homogenized in 1.2 mL of pre-cooled (-20°C) 70% methanol solution supplemented with internal standards. The internal standard solution was formulated by dissolving 1 mg of the reference compound in 1 mL of 70% methanol, yielding a stock concentration of 1,000 μg/mL. The solution was subsequently diluted to 250 μg/mL using 70% methanol. The sample was vortexed for 30 seconds at half-hour intervals, completing six cycles in total, and subsequently centrifuged at 12,000 rpm for 3 minutes. Afterward, the supernatant

obtained was filtered through a 0.22 μm microporous membrane before being subjected to UPLC-MS/MS analysis.

Chromatographic separation was performed using 0.1% formic acid in ultrapure water (Solvent A) and 0.1% formic acid in acetonitrile (Solvent B). The gradient elution, delivered at 0.35 mL/min, was as follows: 0.0-9.0 min, 5% to 95% B (linear); 9.0-10.0 min, 95% B (isocratic); 10.0-11.0 min, 95% to 5% B (linear); 11.0-14.0 min, 5% B (re-equilibration). The column temperature was maintained at 40°C, and the injection volume was 2 μL.

Data acquisition and spectrometric evaluation were performed using Analyst 1.6.3 software. Qualitative and quantitative assessments were performed against an in-house metabolic database. Characteristic ions for each compound were selected via triple quadrupole filtration, with signal intensities (counts per second, CPS) recorded by the detector. Raw spectral files were processed in MultiQuant software for chromatographic peak integration and baseline correction. The relative amount of each compound was determined by calculating the integrated area under the peaks. Final datasets containing all chromatographic peak area integrations were exported and archived.

Obtaining targets associated with SFs and HCC

Active compounds were selected using TCMSP (https://old.tcmsp-e.com/tcmsp.ph) based on pharmacokinetic parameters, including oral bioavailability exceeding 30% and drug-likeness greater than 0.18. Subsequently, related targets were identified and normalized to gene symbols utilizing the UniProt database (https://www.uniprot.org/). Genes associated with oxidative stress (OS) were retrieved from GenCards (https://www.genecards.org/), while additional target genes were sourced from the OMIM database (https://www.omim.org/). The target genes in the two databases were merged and deduplicated. Overlapping targets between SFs and OS were identified using the Venn package.

Constructing protein-protein interaction network (PPI)

The treatment targets related to oxidative stress were identified by intersecting the SFs targets with genes linked to oxidative stress. The shared genes were further examined through the STRING 11.0 platform (https://string-db.org/), specifying Homo sapiens as the species and applying a combined interaction score cutoff greater than 0.9. Following the exclusion of unconnected targets, PPI network was systematically constructed to visualize functional associations. The network was imported into Cytoscape 3.9.1 for topology analysis. MCODE clustering (K-core = 2, node score cutoff = 0.2) partitioned the network into 45 subnetworks. The highest-scoring subnetwork (MCODE score) was prioritized for CytoHubba analysis using Maximal Clique Centrality (MCC), identifying hub genes.

Gene ontology (GO) enrichment analysis

GO enrichment, including molecular function (MF), cellular component (CC), and biological process (BP), was performed via the ClusterProfiler package with GO database (https://www.geneontology.org/). Parameters included human species, p-value ≤ 0.05 (FDR-corrected), and gene set max size limits (500).

Kyoto Encyclopedia of Genes and Genomes (KEGG) pathway enrichment analysis

KEGG enrichment analysis is based on the KEGG (https://www.genome.jp/kegg/) database, combining data on differential genes, proteins, or metabolites to explore their enrichment in specific biological pathways, thereby revealing the underlying mechanisms of related biological processes between SFs and OS. KEGG pathway analysis using ClusterProfiler identified top 20 enriched pathways (p-value ranked). Key pathways included MAPK signaling and PI3K/Akt signaling, visualized via ggplot2.

Molecular docking

JAK2 and PIK3CA were identified as central targets due to exhibiting the greatest degree of node connectivity within the interaction network in the PPI network associated with oxidative stress and sea buckthorn flavonoid components. As the catalytic subunit of PI3K, PIK3CA mediates PI3K pathway activation and regulates cellular proliferation and survival. Molecular docking was performed using the 3D structures of sea buckthorn flavonoids retriev-

ed from the PubChem database (https://pubchem.ncbi.nlm.nih.gov) and target protein structures (PDB IDs: 7L1C for PIK3CA, 7TEU for JAK2, 1ALU for IL-6) downloaded from the Protein Data Bank (https://www.rcsb.org). AutoDock Vina served as the computational tool for evaluating the binding scores of the compounds (chrysin, hesperetin, acacetin and nobiletin) and proteins (JAK2, PIK3CA, IL-6). Protein models were prepared using PyMOL, during which all ligands and water molecules were eliminated as part of the preprocessing steps. Docking simulations between the two targets and sea buckthorn flavonoids (acacetin, hesperetin, nobiletin, and chrysin) were performed with the aid of AutoDock Vina (v1.1.2, developed by the Scripps Research Institute, USA) and PyMOL (version 3.1.3, Schrödinger, USA). To optimize binding affinity assessment, docking parameters including XYZ coordinates and grid dimensions were adjusted to identify optimal flexible docking conditions.

Molecular dynamics simulations

GROMACS 2023.3 software was employed to carry out molecular dynamics simulations to investigate the stability of protein-ligand complexes identified through molecular docking [18]. The docking study utilized sea buckthorn flavonoid structures from PubChem and target proteins (PIK3CA: 7L1C, JAK2: 7TEU) from the Protein Data Bank. The AMBER14SB force field was applied to proteins while GAFF parameters described ligands, with topology files generated using ACPYPE [19]. Systems were solvated in TIP3P water within a 1.2 nm cubic box and neutralized with Na^+/Cl^-. Energy minimization employed the conjugate gradient method until convergence (max force < 10 kJ/mol/nm). Subsequent equilibration included 100 ps NVT phase at 300 K (V-rescale thermostat) and 100 ps NPT phase at 1 atm (Parrinello-Rahman barostat), using 2 fs timestep with LINCS bond constraints. Long-range electrostatics were handled by PME with 1.2 nm cutoffs. Production simulations extended for 100 ns under NPT conditions. Trajectories were analyzed using GROMACS tools for 3D free energy landscape, Radius of Gyration (Rg), Root Mean Square Deviation (RMSD), Root Mean Square Fluctuation (RMSF), Solvent Accessible Surface Area (SASA), and hydrogen bonding (distance < 0.35 nm, angle > 120°), with visualization performed in VMD.

ABTS assay

The antioxidant capacity of SFs and vitamin C was evaluated using the Total ABTS Antioxidant Capacity Assay Kit (S0119, Beyotime, China). First, the ABTS•$^+$ working solution was prepared by incubating the ABTS stock with the provided oxidant reagent in the dark at room temperature for 12 hours. The ABTS•$^+$ solution was subsequently diluted using ethanol to achieve an absorbance value of 0.70 ± 0.05 at 734 nm. For each assay, 10 μL of appropriately diluted sample was added to 200 μL of the ABTS•$^+$ solution; after reacting for 6 minutes at room temperature, the decrease in absorbance at 734 nm was recorded. Radical scavenging activity (%) was calculated as:

$$Clearance\ rate(\%) = (1 - \frac{A_{sample} - A_{blank}}{A_{control}}) \times 100\%$$

DPPH assay

The free radical scavenging ability of SFs and vitamin C was evaluated by employing the DPPH antioxidant capacity assay kit (BC4750, SolarBio, China). A 0.1 mM DPPH solution in ethanol was prepared, and 1 mL of this solution was combined with 100 μL of the sample. The solution was kept in darkness at ambient temperature and allowed to react for 30 minutes. The reduction in DPPH absorbance was determined at 517 nm with a UV-Vis spectrophotometer (UV-1800, Shimadzu, Japan). The radical scavenging capacity was then calculated following the formula applied in the ABTS assay.

Determination of free radical scavenging ability using fenton reaction (PSC)

The ability of SFs to scavenge hydroxyl radicals, generated by the Fenton reaction in a pH 7.4 phosphate buffer, was quantified using an assay kit (Elascience, E-BC-K527-M, China). The reaction mixture comprises 2-deoxy-D-ribose (0.28% w/v), a ferrous ion source (100 μM $FeSO_4$), and 1 mM H_2O_2, along with varying concentrations of SFs and Vc (10 μg/mL, 50 μg/mL and 100 μg/mL). Samples were incubated at 37°C for 60 minutes to allow for radical-induced breakdown of 2-deoxy-D-ribose. The reaction was stopped with an equal volume of a 1% thiobarbituric acid (TBA) and 2.8% trichloroacetic acid (TCA) mixture. To activate the chromophore, samples were heated at 100°C

for 15 minutes before the absorbance was read at 532 nm on a UV-Vis spectrophotometer.

Measurement of superoxide radical scavenging ability using the xanthine oxidase method (TOAC assay)

The Total Antioxidant Capacity Assay Kit (Yeasen, China) was employed to evaluate the ability of SFs to scavenge superoxide radicals. Superoxide anions (O_2^-•) were generated enzymatically by the xanthine/xanthine oxidase system in a pH 7.4 phosphate buffer. The reaction mixture includes xanthine as the substrate, xanthine oxidase to catalyze the oxidation of xanthine, and nitroblue tetrazolium (NBT) as a chromogenic probe. In the absence of a scavenger, the produced O_2^-• radicals reduce NBT to form a colored formazan product, which is monitored spectrophotometrically at 560 nm. SFs and Vc at concentrations of 10, 50, and 100 μg/mL were introduced into the reaction mixture to scavenge O_2^-• radicals.

Cell culture and treatment

HepG2 cells, obtained from the Cell Bank of Type Culture Collection at the Chinese Academy of Sciences (Shanghai, China), were maintained in DMEM (Thermo Fisher Scientific, USA) enriched with 10% fetal bovine serum (Gibco, USA) and antibiotics (100 U/mL penicillin and 100 μg/mL streptomycin; Beyotime, China). Cultures were incubated at 37°C in a humidified atmosphere containing 5% CO_2. For treatment experiments, SFs and vitamin C were applied at concentrations of 10, 50, and 100 μg/mL for 24 hours. Cell supernatants and proteins were collected for subsequent experiments.

CCK-8 assay

Cell proliferation was assessed by the CCK-8 assay (BS350B, Biosharp, China). HepG2 cells were seeded into 96-well plates at 4×10^3 cells per well and allowed to adhere for 24 hours. Subsequently, cultures were exposed to SFs at 10, 50, or 100 μg/mL for another 24 hours. After treatment, 10 μL of CCK-8 reagent was added to each well and incubated at 37°C for 1 hour. Finally, absorbance was measured at 450 nm using a microplate reader (Agilent BioTek Epoch 2, Agilent, USA).

Flow cytometry analysis

Following treatment, HepG2 cells were rinsed twice with ice-cold PBS to eliminate remaining culture medium. The cells were subsequently resuspended in 1 × Annexin V binding buffer (Elabscience, China) at a density of approximately 1×10^6 cells/mL. One hundred microliters of cell suspension were placed into flow cytometry tubes and incubated with 5 μL of Annexin V-FITC solution for 15 minutes at room temperature in the dark to permit phosphatidylserine binding. Before conducting flow cytometry, each tube received 5 μL of propidium iodide (PI) solution (Elabscience, China) and was subsequently incubated in the dark for 5 minutes. Finally, 400 μL of 1 × binding buffer was added to adjust sample volume, and all specimens were maintained on ice until analysis. Fluorescence signals were quantified using a Beckman flow cytometer (Beckman, USA) with standard configuration for FITC/PI detection.

Enzyme-linked immunosorbent assay (ELISA)

IL-6, TNF-α and COX-2 levels were measured using commercial IL-6 ELISA kit (EK106/2-AW1, LiankeBio, China), TNF-α ELISA kit (EK182HS-AW1, LiankeBio, China), and COX-2 ELISA kit (ml062904, MIBio, China). A 96-well microplate was incubated overnight at 4°C after being coated with 50 μL of capture antibodies specific for IL-6, TNF-α, and COX-2. Following this, the wells were rinsed three times using a standard washing buffer. Subsequently, 100 μL of HRP-labeled secondary antibody was introduced into each well and allowed to react for 1 hour at room temperature. After a further wash, 90 μL of TMB substrate was introduced, the reaction was halted with stop solution, and the optical density at 450 nm was recorded using a microplate spectrophotometer (BioTek, USA).

Real-time quantitative PCR (RT-qPCR)

Total RNA was extracted from HepG2 cells using the TransZol Up Plus RNA Kit (ER501-01, TRANS, Switzerland) according to the manufacturer's instructions. cDNA was synthesized using the One-Step gDNA Removal (AU341, TRANS, Switzerland) following the manufacturer's protocol. RT-qPCR was performed using MagicSYBR Mixture (CW3008, ConwayCentury, China). The amplification program was as follows: The PCR protocol began with an initial

Table 1. The primer sequences for qRT-PCR

Primers	Sequence (5'→3')
PI3KCA-F	5'-GAAGCACCTGAATAGGCAAGTCG-3'
PI3KCA-R	5'-GAGCATCCATGAAATCTGGTCGC-3'
AKT-F	5'-TGGACTACCTGCACTCGGAGAA-3'
AKT-R	5'-GTGCCGCAAAAGGTCTTCATGG-3'
JAK2-F	5'-CCAGATGGAAACTGTTCGCTCAG-3'
JAK2-R	5'-GAGGTTGGTACATCAGAAACACC-3'
GAPDH-F	5'-GGAGCGAGATCCCTCCAAAAT-3'
GAPDH-R	5'-GGCTGTTGTCATACTTCTCATGG-3'

denaturation step at 95°C for 10 minutes, followed by 40 amplification cycles consisting of 95°C for 10 seconds and 60°C for 30 seconds. Relative quantification of gene expression was performed using the $2^{-\Delta\Delta Ct}$ approach, with GAPDH serving as the reference gene. The primers used for the target and reference genes are listed in **Table 1**.

Western blot

Proteins were isolated from HepG2 cells using RIPA lysis buffer (R0010, Solabio, China) supplemented with 1% protease inhibitor cocktail (P1005, Beyotime, China). Protein concentrations were quantified using the BCA assay kit (BL521S, Biosharp, China). Equivalent quantities of protein samples were separated via 10% SDS-PAGE and subsequently transferred to PVDF membranes (IPVH00010, Millipore, USA) using the Trans-Blot Turbo transfer apparatus (Bio-Rad, USA). The membranes were first incubated in TBST containing 5% nonfat milk at room temperature for 1 hour to block nonspecific binding, followed by an overnight incubation at 4°C with the designated primary antibodies. PI3K (1:1,000; Invitrogen, PA5-29220), p-AKT (1:1,000; Proteintech, 28731-1-AP), AKT (1:1,000; Cohesion, CPA1034), p-JAK2 (1:1,000; Proteintech, 17670-1-AP), and JAK2 (1:1,000; Proteintech, 29101-1-AP). After three TBST washes, HRP-conjugated secondary antibody (1:5,000; Proteintech, SA00001-2) was applied for 1 hour at room temperature. Signal detection was performed using an ECL system (Tanon-5200, Tianeng, China), and band densities were quantified with ImageJ. β-Actin (1:1,000; Proteintech, USA) served as a loading control.

Statistical analysis

Statistical analysis was performed using GraphPad Prism 8 software (v8.0.1). All data were expressed as mean ± standard deviation (SD) from at least three independent experiments. Comparisons between two groups were analyzed using an unpaired Student's t-test. Comparisons among more than two groups were analyzed using a one-way analysis of variance (ANOVA) followed by Dunnett's multiple comparisons test to compare each treatment group against the designated control group. A *P*-value < 0.05 was considered statistically significant.

Results

Component analysis of SFs

SFs can be isolated via counter-current chromatography and mechanochemical-assisted extraction, but a customized extraction protocol with optimized parameters was developed and systematically employed in this study. The extraction conditions were: ethanol concentration of 50%, extraction temperature of 60°C, extraction time of 40 min, ammonium sulfate 1.25 g/20 mL, and flavonoid extraction rate of 529.91 mg/100 g. In this study, ultrasonication-assisted ammonium sulfate-ethanol extraction was employed for phytochemical isolation, followed by LC-MS-based separation and characterization. Based on the local metabolic database, the compounds of the samples were analyzed by mass spectrometry qualitatively and quantitatively, which identified 1,988 compounds: 695 flavonoids, 427 terpenoids, 223 phenolic acids, 219 alkaloids, 140 lignans/coumarins, 31 quinones, 25 tannins, 11 steroids, and 217 miscellaneous compounds. The flavonoids in the top 10 include chrysin, hesperetin, acacetin and nobiletin (**Figure 1**).

Network pharmacology analysis

To investigate potential molecular targets of SFs for oxidative stress, network pharmacology analysis was used. The keyword "Oxidative Stress" was entered into the GeneCards database to collect disease targets, filtered by excluding genes with scores below the median (3.2014), yielding 7072 targets. A total of 73 relevant genes were retrieved from the OMIM (Online Mendelian Inheritance in Man) database. The target genes in the two databases were merged and deduplicated, and 7144 genes were finally obtained. The results are shown in the Venn diagram (**Figure 2A**). The interplay between SFs and oxidative stress tar-

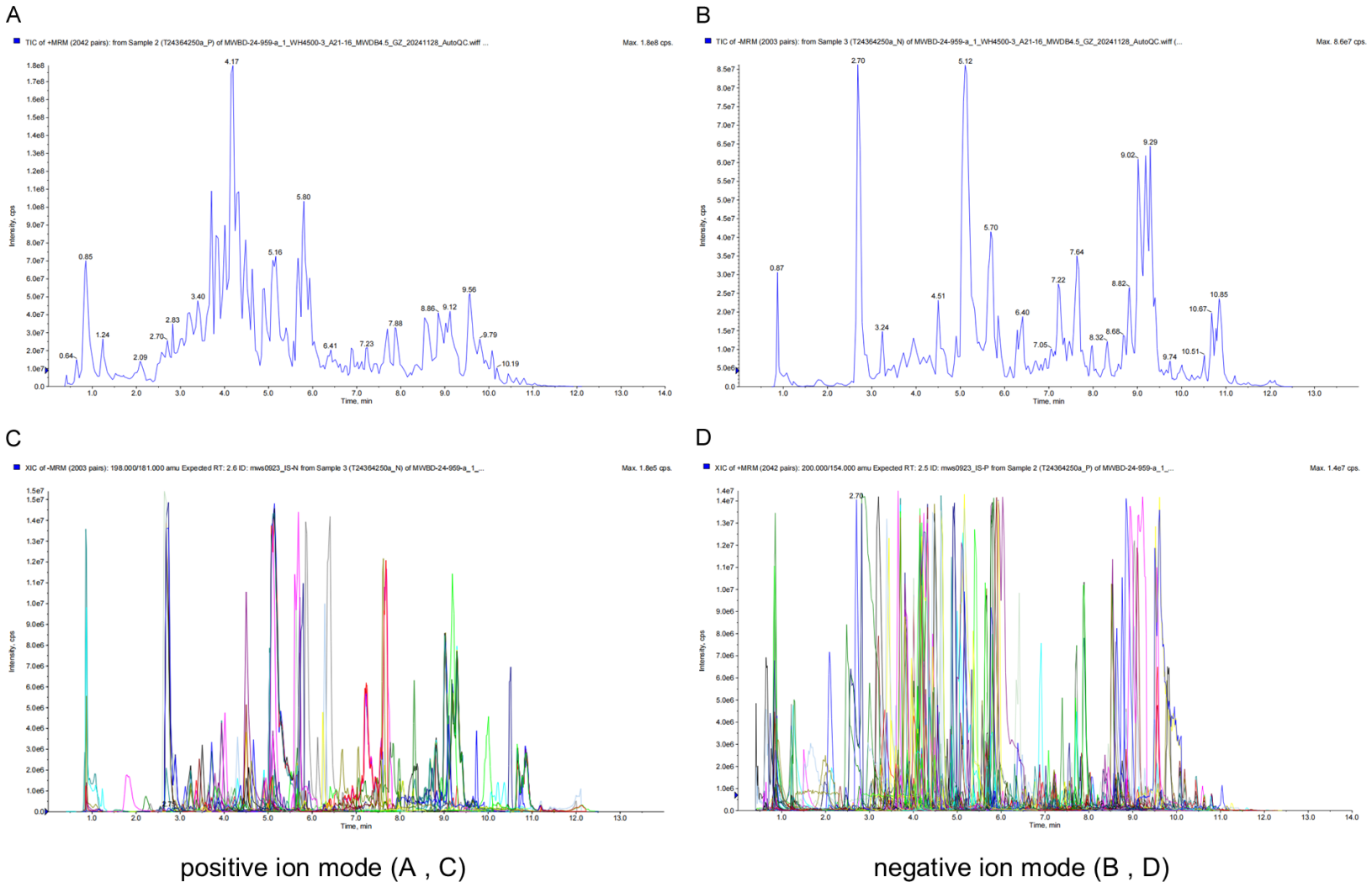

Figure 1. LC-MS analysis of SFs. The total ion chromatograms (TIC, representing the summed ion intensity across all detected m/z values at each time point) and multiple reaction monitoring (MRM) chromatograms (extracted ion chromatograms, XIC) of SFs are displayed in both positive and negative ion modes. The x-axis indicates retention time (RT, min), while the y-axis represents ion intensity (counts per second, cps). SFs were separated and detected by LC-MS, followed by qualitative and quantitative analysis using an in-house metabolic database. A. TIC in positive ion mode; B. TIC in negative ion mode; C. MRM chromatograms (XIC) in positive ion mode; D. MRM chromatograms (XIC) in negative ion mode.

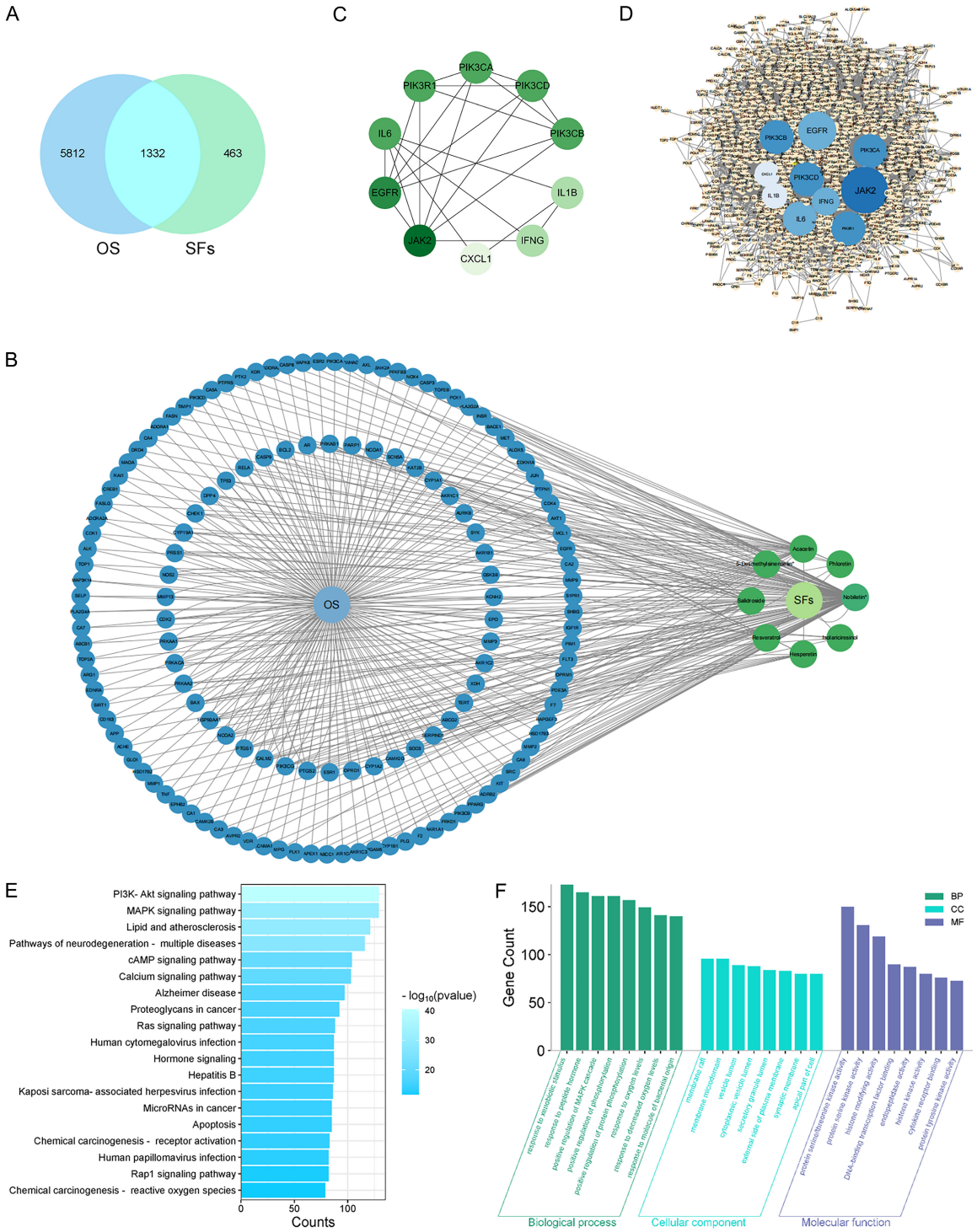

Figure 2. Network pharmacology analysis of potential targets for SFs in oxidative stress. The targets of SFs and oxidative stress were obtained by the TCSMP database and the GenCard database, respectively. Then, PPI network was constructed, and therapeutic pathways were predicted by GO enrichment and KEGG pathway enrichment analysis. A. Venn diagram illustrating the common targets between SFs and oxidative stress. B. The interrelationship of SFs and oxidative stress targets. C. PPI network identifying key disease targets. D. The interrelationship of key disease targets. E. KEGG pathway analysis revealing the major biological pathways associated with the common targets of SFs and OS (oxidative stress). F. GO analysis highlighting the enrichment of these targets in BP, MF, and CC.

gets is presented in **Figure 2B**. PPI network constructed using the STRING database contained 1,211 nodes and 6,359 edges. Subsequent PPI analysis identified the top 10 hub genes: JAK2, EGFR, IL6, PIK3R1, PIK3CA, PIK3CD, PIK3CB, IL1B, IFNG, and CXCL1 (**Figure 2C**). The interconnections among these hub genes were illustrated, revealing the most extensive interactions between JAK2 and other hub genes (**Figure 2D**).

KEGG pathway analysis identified significant enrichment in key signaling pathways, including PI3K/Akt, MAPK, and Ras. The PI3K/Akt pathway showed the greatest number of associated genes, which is consistent with the PPI analysis. Other enriched pathways included cancer-associated microRNA regulation, receptor-mediated and ROS-driven chemical carcinogenesis, and tumor-associated proteoglycan signaling (**Figure 2E**).

The GO analysis implicated hypoxic stress as a central driver, with top BP terms including "response to oxygen levels" and "response to decreased oxygen levels". This stress was functionally linked to the "positive regulation of MAPK cascade", suggesting that cells respond to oxidative conditions by activating this key pathway, which is consistent with the broader engagement of pro-survival (PI3K/Akt) and NF-κB signaling. The CC analysis localized these events, identifying enrichment for "membrane raft" and "cytoplasmic microdomain", which are key signaling hubs on the cell surface. Furthermore, terms like "vesicle lumen" and "secretory granule lumen" suggest that ROS may also exert effects within the endomembrane system. The MF analysis was dominated by kinase and regulatory activities, including "protein serine/threonine kinase", "protein tyrosine kinase" and "histone kinase" functions, as well as "histone modification" (**Figure 2F**).

Interaction intensity of chrysin, hesperetin, acacetin and nobiletin docking with JAK2 or PIK3CA

To elucidate binding mechanisms, we docked the active compounds (chrysin, hesperetin, acacetin, and nobiletin) against JAK2 or PIK3CA. This analysis succeeded in quantifying their binding energies and identify key intermolecular interactions. All four compounds displayed high predicted binding affinities for targets, yielding significantly lower binding energies than IL-6. Besides, the compounds showed stronger binding capabilities to JAK2 than to PIK3CA, particularly chrysin-JAK2 and acacetin-JAK2 complexes, which achieved stronger binding capabilities (the binding energies = -8.8 kcal/mol) (**Figure 3A**). Based on these findings, four top complexes in JAK2 group and a top complex in PIK3CA group were selected for further molecular docking visualization.

Hydrogen bonding emerged as the primary interaction mechanism linking active compounds to their protein targets. The acacetin-JAK2 complex formed dual hydrogen bonds between its benzopyran ring phenolic hydroxyl group and ASP-997 residues. Chrysin established two hydrogen bonds via its phenolic hydroxyl groups with LEU-932 of JAK2. This potentially explains their strong binding affinity. Hesperetin exhibited hydrogen bonding between its benzopyran ring hydroxyl group and JAK2's LEU-932, along with dual interactions between its methoxy group and ASP-994. In the nobiletin-JAK2 complex, hydrogen bonds were observed between the carbonyl group and LEU-932, as well as between a methoxy group and GLY-856. Additionally, nobiletin-PIK3CA interactions involved multiple hydrogen bonds: the carbonyl group with VAL-9 and LYS-94, a benzopyran methoxy group with GLN-8, and a benzene ring methoxy group with SER-11 and ARG-234 (**Figure 3B**). These findings collectively demonstrate that chrysin, hesperetin, acacetin, and nobiletin achieve stable binding with JAK2 or PIK3CA primarily through hydrogen bonding networks.

Molecular dynamics simulation of Flavonoid-JAK2 complexes

Molecular dynamics simulations showed that all of the four flavonoids (Acacetin, Chrysin, Hesperetin and Nobiletin) formed dynamically stable complex with JAK2 with low energy conformational states, maintained hydrogen bonding and also provided dynamic structural changes. However, although each of the four flavonoids formed complexes with JAK2 thermodynamically, there was great variance in their dynamic behaviors. Acacetin exemplified a rigid binding mode; Acacetin demonstrated rapid structural equilibrium (RMSD stabilized < 10 ns at 0.2-0.4

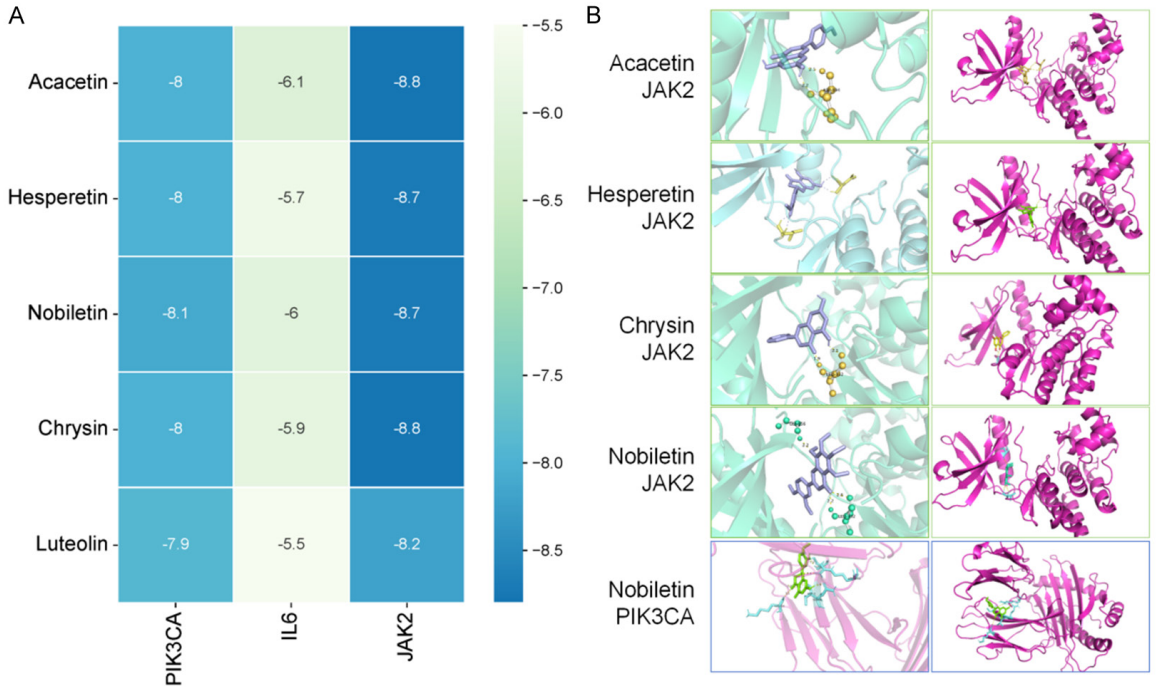

Figure 3. Molecular docking of flavonoids (chrysin, hesperetin, acacetin, and nobiletin) with target proteins JAK2 or PIK3CA. Binding energies were calculated using the scoring function of AutoDock Vina. Docking simulations and structural visualizations were performed with PyMOL and AutoDock Vina. A. Calculated binding energy values for ligand-protein interactions. B. Two and three-dimensional representations of docking poses, highlighting critical binding residues.

nm) and was trapped by the presence of tenacious hydrogen bonds (1-2) and low residue flexibility (RMSF: 0.1-0.4 nm). Chrysin was a fit that was intermediate and dynamic. It took more time to reach equilibrium (~20 ns) and displayed increased hydrogen bond transitions (1-3 bonds) and intermediate RMSD oscillations (0.2-0.6 nm) (**Figure 4**).

By comparison, Hesperetin and Nobiletin were very adaptable. Both complexes showed strong changes in their RMSD (with a maximum RMSD fluctuation of 0.8 nm), highly fluctuating hydrogen bonds (0-6 bonds), and a strong degree of functionality flexibility (residues 850-900, 1000-1050; RMSF: up to 0.4 nm). Such findings allowed identifying Acacetin as a static rigid binder, whereas Hesperetin and Nobiletin seemed to be more energetic, dynamic ligands that explored the binding pocket on a large scale (Figure S1).

The antioxidant effect of SFs

To reveal the antioxidant capacity of SFs, we used four distinct assays, including DPPH, ABTS, PSC, and TOAC, to assess it. In the DPPH and ABTS radical scavenging assays, SFs showed clear dose-dependent activity but were less potent than Vc (**Figure 5B**, **5C**). The weaker DPPH response, in particular, may be a technical problem of preferential solubility of DPPH, rather than a true reflection of efficacy (**Figure 5B**).

In contrast, SFs were comparable to Vc in the PSC and TOAC assays. The PSC assay, which measures hydroxyl radical (OH•) scavenging, showed nearly identical performance (**Figure 5A**). Similarly, in the TOAC assay, SFs at 100 μg/mL achieved the same maximal scavenging rate as Vc (**Figure 5D**). This suggests that while Vc reaches its peak antioxidant capacity at lower concentrations, SFs can catch up and offer equivalent total capacity in these specific systems.

The effect of SFs on cell viability and apoptosis

We assessed the impact of SFs on HepG2 cell viability and apoptosis using CCK-8 assays and flow cytometry. SFs decreased cell viability in a

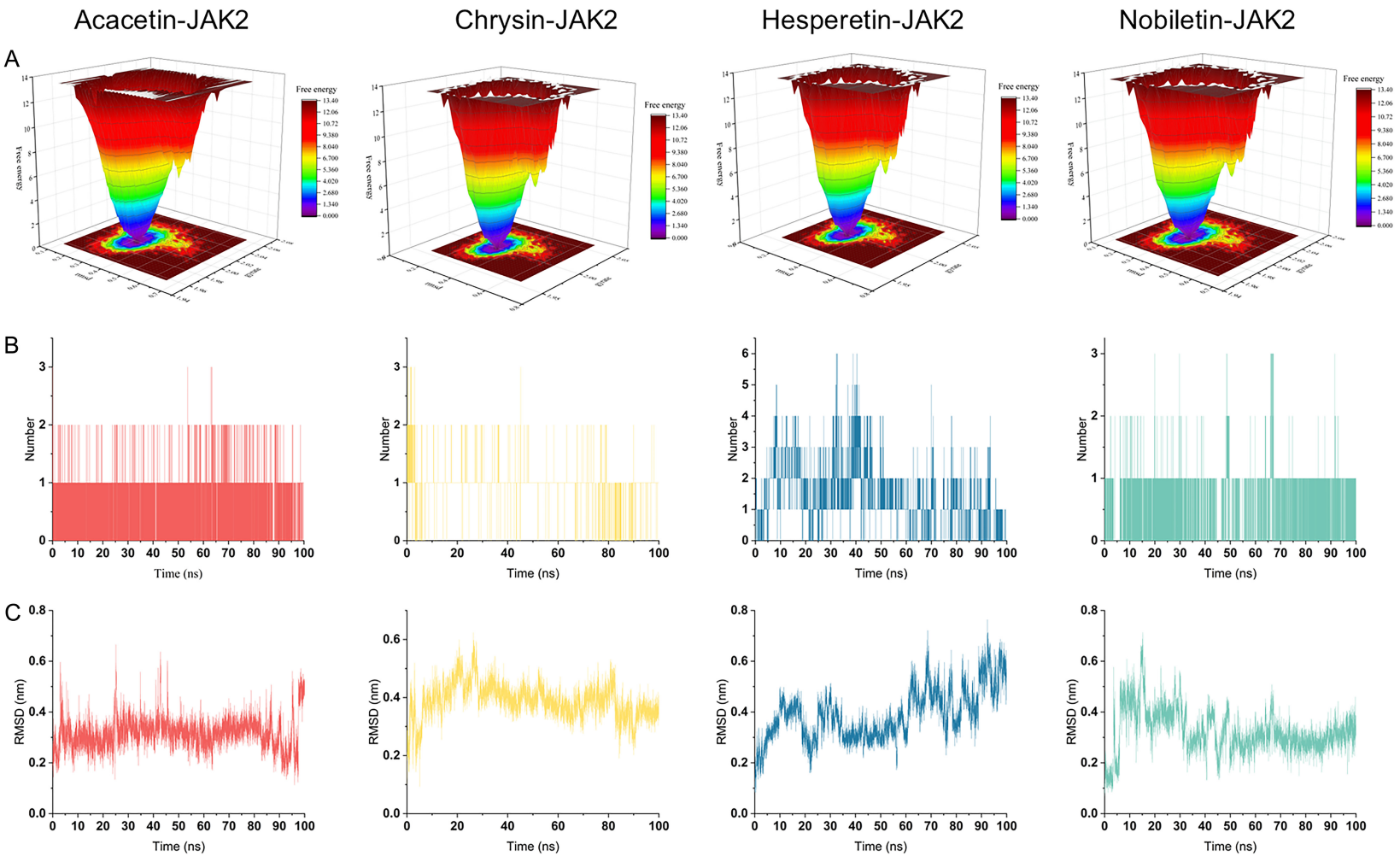

Figure 4. Comparative molecular dynamics analyses of flavonoid-JAK2 complexes. Molecular dynamics simulations (GROMACS) using AMBER14SB/GAFF force fields evaluated docked flavonoid-protein complexes through system solvation, energy minimization, NVT/NPT equilibration, and stability analyses (3D free energy landscape, RMSD, RMSF, Rg, SASA, hydrogen bonds). A. Overlay of free energy landscapes for Acacetin (blue), Chrysin (green), Hesperetin (orange), and Nobiletin (red), highlighting low-energy basins. B. Hydrogen bond frequency distributions. C. RMSD trajectories showing equilibration.

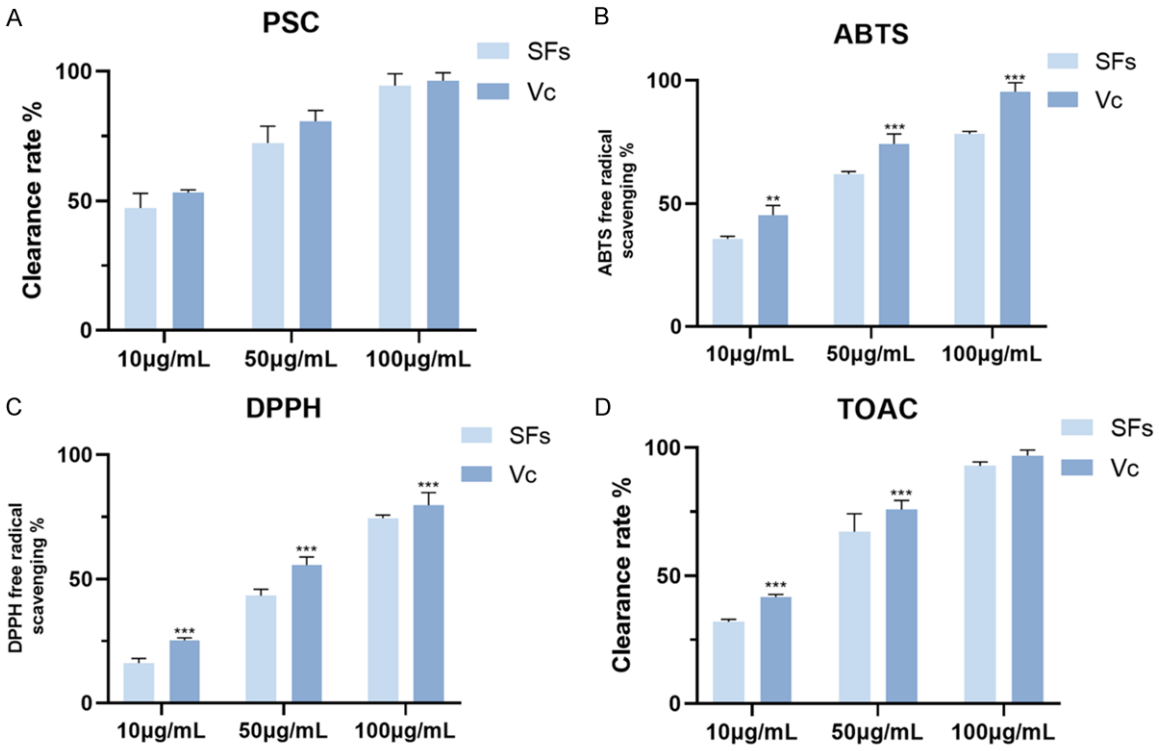

Figure 5. Antioxidant capacity of SFs and Vc assessed by PSC, ABTS, DPPH, and TOAC assays. A. Hydroxyl radical (OH•) scavenging capacity reflecting oxidative damage mitigation in PSC assay. B. Total antioxidant capacity evaluated via ABTS assay. C. Stable free radical scavenging activity measured by DPPH assay. D. Superoxide anion radical (O_2^-•) scavenging capacity measured by TOAC assay. Results are represented as means ± standard deviations for at least three independent experiments. Statistical significance is indicated as follows: ***P < 0.001, SFs vs. Vc group.

dose-dependent manner, and 10 μg/mL reduced viability to approximately 80%, while both 50 and 100 μg/mL reduced it below 50% (**Figure 6A**). Apoptosis rates remained at a low level at 10 and 50 μg/mL but rose significantly at 100 μg/mL (**Figure 6B**, **6C**). Therefore, we selected 10 μg/mL for all subsequent cellular experiments. This concentration is clearly bioactive but is low enough to avoid the confounding, non-specific cytotoxicity observed at higher doses.

PI3K/Akt and JAK signaling pathways were inhibited by SFs in HepG2 cells

IL-6, TNF-α, and COX-2 are key cytokines regulated by the PI3K/Akt and JAK signaling pathways. Therefore, prior to examining the PI3K/Akt and JAK pathways, we first assessed the effects of SFs on these cytokines. The results demonstrated that SFs reduced the levels of IL-6, TNF-α, and COX-2 in HepG2 cells in a concentration-dependent manner (**Figure 7A-C**).

Furthermore, we evaluated the expression of PIK3CA and the phosphorylation levels of AKT and JAK2, and found that SFs markedly decreased PIK3CA protein abundance as well as the phosphorylation of AKT and JAK2 (**Figure 7D-G**). Meanwhile, SFs also decreased mRNA levels of PIK3CA, AKT, and JAK2 (**Figure 7H-J**). Taken together, these results suggest that SFs regulate the PI3K/Akt and JAK signaling cascades at transcriptional and post-translational stages.

Discussion

Flavonoids are natural polyphenols characterized by antioxidant behaviors and wide spectrum of biologic characteristics such as antibacterial effects, anti-inflammatory effects, and so on contributing to low risk of the disease [20]. To extract flavonoids of sea buckthorn, in this research, we have used ultrasonication aided aqueous two-phases system. This method offers advantages over conventional reflux,

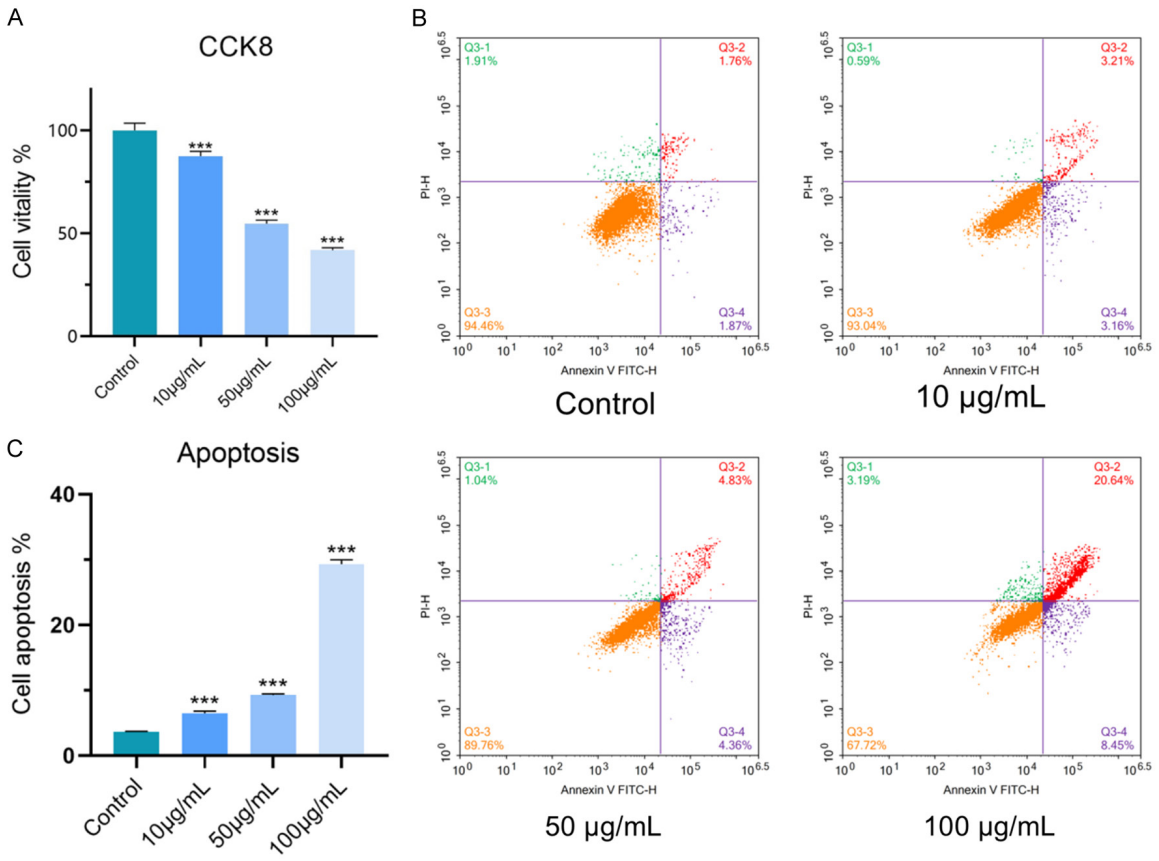

Figure 6. CCK-8 and flow cytometry assay were used to determine the optimal concentration of SFs in HepG2 cells. The cells were treated with different concentrations of SFs (10, 50, 100 μg/mL). A. CCK-8 results showing cell viability at different concentrations. B. Gate diagram of cells in flow cytometry. C. The percentage of apoptotic cells (Q3-2 + Q3-4). Data are presented as the mean ± SD of at least three independent experiments. ***$P < 0.001$ compared with the control group.

maceration, and Soxhlet extraction techniques. While traditional methods are time-consuming, ultrasonic waves facilitate cell wall disruption, thereby significantly shortening the extraction time [21]. Moreover, the aqueous two-phase system makes the separation process easier through the enriched flavonoids in the alcohol phase due to the partition coefficients [22]. Using network pharmacology, we then detected a connection between SFs and oxidative stress, and thus theorized that the connection can take place through the PI3K/Akt and JAK signaling pathways. One of the known causes of HCC is oxidative stress. There exists a significant amount of evidence indicating the presence of the hepatoprotective effect in antioxidant compounds including ascorbic acid, lipoic acid, and quercetin [23] that might be employed in HCC treatment. Thus, we explored the development of SFs as anti-cancer agents based on their antioxidant property and confirmed their mechanism of action.

In order to evaluate the antioxidant activity of SFs accurately, four different tests were used, namely, DPPH, ABTS, PSC, and TOAC assay. Even though the quantified antioxidant capacity between the different approaches was slightly different, overall, the findings indicate that SFs have a considerable antioxidant activity. After this verification, we researched on the mechanism involved. Our analysis revealed that there are four different SF elements that interact with critical targets. Namely, chrysin and acacetin had a high and stable binding model with JAK2, but hesperetin and nobiletin showed other conformational types of flexibility during their interactions with PIK3CA. Guo et al. and Wang et al. were able to use the hepatoprotective and antioxidant properties of the SFs in a previous

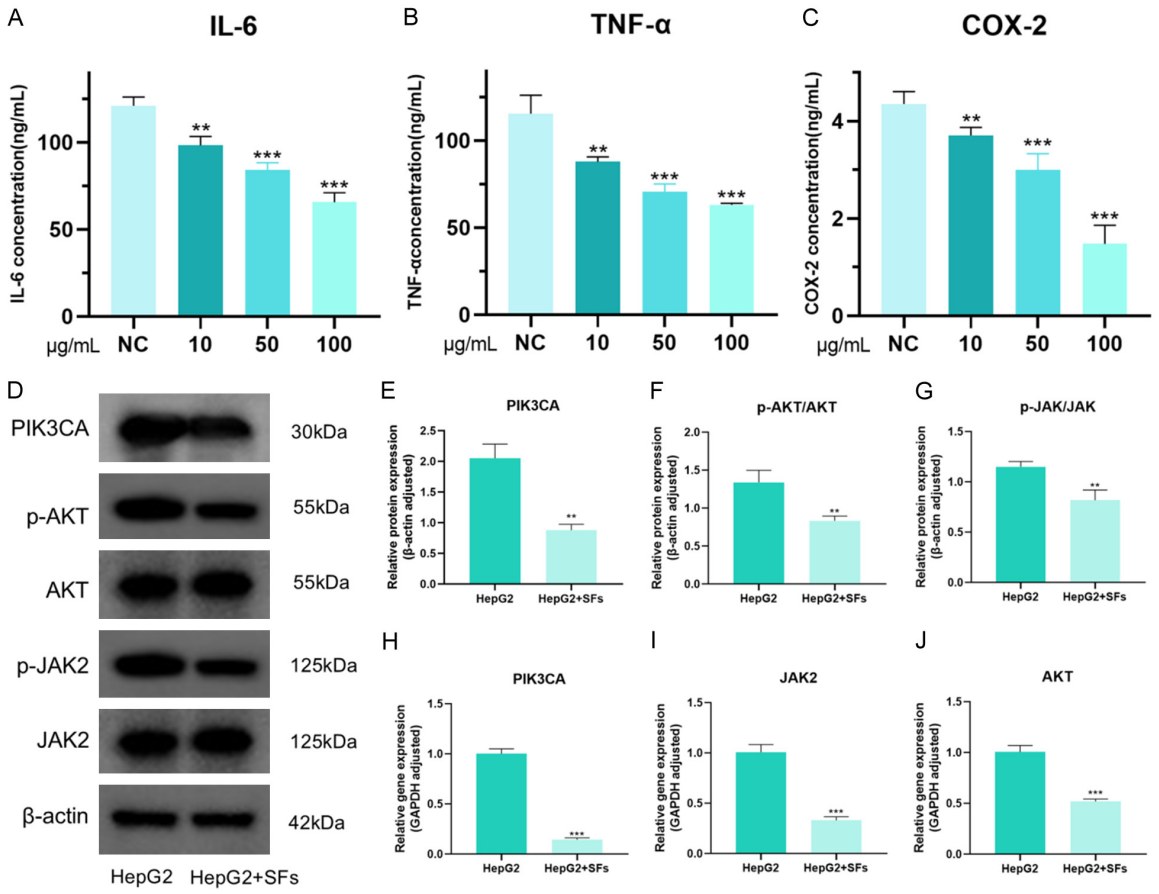

Figure 7. SFs regulate PI3K/Akt and JAK signaling pathway. NC, normal control. HepG2 cells were treated with SFs (10 μg/mL) for 24 h, then the protein and mRNA were extracted and tested. A-C. Levels of IL-6, TNF-α, and COX-2 after treatment with 10 μg/mL, 50 μg/mL and 100 μg/mL SFs for 24 h. $^{**}P < 0.01$, $^{***}P < 0.001$ compared with NC group. D. Representative Western blot images for PIK3CA, p-AKT, AKT, p-JAK2, and JAK2. β-actin was used as a loading control. E-G. Quantification of relative protein expression from Western blots. H-J. Relative mRNA expression levels of PIK3CA, AKT1, and JAK2 determined by RT-qPCR. Data are presented as the mean ± SD (n = 3). $^{**}P < 0.01$, $^{***}P < 0.001$ compared with the HepG2 group.

study, respectively, but did not specifically focus on attributes of these properties to the treatment of HCC [24, 25]. In comparison, the present study provided a more detailed and more extensive virtual simulation of the interactions between SFs and their therapeutic targets.

We further confirmed the inhibitory effect of SFs on PI3K/Akt and JAK signaling pathways in liver cancer cells at the cellular level of gene and protein expression. The previous study by Xia et al. found that PI3K/Akt is inhibited by SFs, though they did not study the neurotrophic roles of SFs in the treatment of brain diseases [26]. Equally, Wang et al. indicated that SFs protect endothelial cells against oxidative inflammation through PI3K/Akt-eNOS route [27]. Our work incorporates these ideas, but puts special emphasis on the use of SF-mediated antioxidant activities in HCC and, in such a way, it will increase the therapeutic application of SFs in medicine. Moreover, there are also some flavonoid monomers in sea buckthorn, which suppress PI3K/Akt. An example of this would be that Isorhamnetin prevents the proliferation and metastasis of human gallbladder cancer cells by hindering PI3K/Akt signaling [28]. Similarly, Quercetin inhibits the development of cholangiocarcinoma cells by blocking JAK signaling pathway and rescues the up-regulation of iNOS and ICAM-1 [29]. However, unlike monomers, SFs can employ their multi-component characteristic and simultaneously activate the PI3K/Akt and JAK pathways, which may have a more potent anti-tumor effect.

Despite the fact that the anti-tumor mechanisms of SFs in this research have been explained depending on their antioxidant capability, it is important to mention several limitations. To start with, the extraction methodology should be further optimized. Although our procedure was successful (529.91 mg/100 g), the composition of the specific flavonoid compared with different extraction methods largely relies on the mode of extraction method. Consequently, the biological activity that was observed, in this case, may not be exactly recreatable with the products that are extracted using alternative methods. Comparative studies with our results need to be conducted in future studies in terms of other methods, like mechanochemical-assisted extraction (MCAE), which can yield higher results [30], or Natural Deep Eutectic Solvents (NADES)-UAE, which is a more environmentally-friendly method [28]. The comparison of SFs extracted using these various methods would explain the correlation between methods of extraction, composition, and anti-tumor activity.

Secondly, there is a restriction of our findings due to the use of the HepG2 cell line. Complex in vivo pharmacokinetics, bioavailability, and other cell-type interactions can not be completely represented in vitro in mechanistic models. The weakness of the study is that there were no extensive in vivo pharmacokinetic studies as well as toxicology tests. This is especially so considering the fact that a large number of flavonoids are known to be relatively unbioavailable [31]. The other limitation is that the SF extract is complex chemically. Our selected compounds were 695 flavonoids but there are thousands of other compounds in the extract. One question remains whether these uninvestigated elements regulate the manifested biological effects and do so via synergy or antagonism mechanisms.

In conclusion, this study highlights the antioxidant-mediated anti-HCC effects of SFs. After verifying the antioxidant capacity of SFs, we utilized network pharmacology, molecular docking, and molecular dynamics simulations to identify key compound-protein interactions. Finally, cellular experiments confirmed at both the protein and gene levels that SFs exert antitumor effects by inhibiting the PI3K/Akt and JAK signaling pathways.

Acknowledgements

This study was supported by the Scientific Research Program of Higher Education Institutions in Inner Mongolia Autonomous Region (NJZY21517), the Agricultural and Livestock Product Processing Science and Technology Innovation Team of Vocational and Technical College of Inner Mongolia Agricultural University (TDY202303) and Special Project for Capacity Construction of National Modern Agricultural Science and Technology Demonstration Bases (RZ2200000482).

Disclosure of conflict of interest

None.

Address correspondence to: Ji Nan, Medical Innovation Center for Nationalities, Inner Mongolia Medical University, Hohhot 010110, Inner Mongolia, China. E-mail: nanji@immu.edu.cn

References

[1] Vogel A, Meyer T, Sapisochin G, Salem R and Saborowski A. Hepatocellular carcinoma. The Lancet 2022; 400: 1345-1362.

[2] Chidambaranathan-Reghupaty S, Fisher PB and Sarkar D. Hepatocellular carcinoma (HCC): epidemiology, etiology and molecular classification. Adv Cancer Res 2021; 149: 1-61.

[3] Siegel RL, Miller KD, Wagle NS and Jemal A. Cancer statistics, 2023. CA Cancer J Clin 2023; 73: 17-48.

[4] Rizzo GEM, Cabibbo G and Craxì A. Hepatitis B virus-associated hepatocellular carcinoma. Viruses 2022; 14: 986.

[5] Kumar R, Goh BBG, Kam JW, Chang PE and Tan CK. Comparisons between non-alcoholic steatohepatitis and alcohol-related hepatocellular carcinoma. Clin Mol Hepatol 2020; 26: 196-208.

[6] Zeng Y, Lian S, Li D, Lin X, Chen B, Wei H and Yang T. Anti-hepatocarcinoma effect of cordycepin against NDEA-induced hepatocellular carcinomas via the PI3K/Akt/mTOR and Nrf2/HO-1/NF-κB pathway in mice. Biomed Pharmacother 2017; 95: 1868-1875.

[7] Ramadan HK-A, Badr G, Ramadan NK and Sayed A. Enhanced immune responses, PI3K/Akt and JAK/STAT signaling pathways following hepatitis C virus eradication by direct-acting antiviral therapy among egyptian patients: a case control study. Pathog Dis 2021; 79: ftab008.

[8] Jelic MD, Mandic AD, Maricic SM and Srdjenovic BU. Oxidative stress and its role in cancer. J Cancer Res Ther 2021; 17: 22-28.

[9] Duan J, Huang Z, Qin S, Li B, Zhang Z, Liu R, Wang K, Nice EC, Jiang J and Huang C. Oxidative stress induces extracellular vesicle release by upregulation of HEXB to facilitate tumour growth in experimental hepatocellular carcinoma. J Extracell Vesicles 2024; 13: e12468.
[10] Liu Z, Ma H and Lai Z. The role of ferroptosis and cuproptosis in curcumin against hepatocellular carcinoma. Molecules 2023; 28: 1623.
[11] Wang X, Qian S, Wang S, Jia S, Zheng N, Yao Q and Gao J. Combination of vitamin C and lenvatinib potentiates antitumor effects in hepatocellular carcinoma cells in vitro. PeerJ 2023; 11: e14610.
[12] Tighe SP, Akhtar D, Iqbal U and Ahmed A. Chronic liver disease and silymarin: a biochemical and clinical review. J Clin Transl Hepatol 2020; 8: 454-458.
[13] Mulati A, Ma S, Zhang H, Ren B, Zhao B, Wang L, Liu X, Zhao T, Kamanova S, Sair AT, Liu Z and Liu X. Sea-buckthorn flavonoids alleviate high-fat and high-fructose diet-induced cognitive impairment by inhibiting insulin resistance and neuroinflammation. J Agric Food Chem 2020; 68: 5835-5846.
[14] Zhou W, Ouyang J, Hu N and Wang H. Flavonoids from hippophae rhamnoides linn. Revert doxorubicin-induced cardiotoxicity through inhibition of mitochondrial dysfunction in H9c2 cardiomyoblasts in vitro. Int J Mol Sci 2023; 24: 3174.
[15] Bao M and Lou Y. Flavonoids from seabuckthorn protect endothelial cells (EA.hy926) from oxidized low-density lipoprotein induced injuries via regulation of LOX-1 and eNOS expression. J Cardiovasc Pharmacol 2006; 48: 834-841.
[16] Igbe I, Shen XF, Jiao W, Qiang Z, Deng T, Li S, Liu WL, Liu HW, Zhang GL and Wang F. Dietary quercetin potentiates the antiproliferative effect of interferon-α in hepatocellular carcinoma cells through activation of JAK/STAT pathway signaling by inhibition of SHP2 phosphatase. Oncotarget 2017; 8: 113734-113748.
[17] Xia CX, Gao AX, Dong TT and Tsim KW. Flavonoids from seabuckthorn (hippophae rhamnoides L.) mimic neurotrophic functions in inducing neurite outgrowth in cultured neurons: Signaling via PI3K/Akt and ERK pathways. Phytomedicine 2023; 115: 154832.
[18] Van Der Spoel D, Lindahl E, Hess B, Groenhof G, Mark AE and Berendsen HJC. GROMACS: fast, flexible, and free. J Comput Chem 2005; 26: 1701-1718.
[19] Kagami L, Wilter A, Diaz A and Vranken W. The ACPYPE web server for small-molecule MD topology generation. Bioinformatics 2023; 39: btad350.
[20] Shen N, Wang T, Gan Q, Liu S, Wang L and Jin B. Plant flavonoids: classification, distribution, biosynthesis, and antioxidant activity. Food Chem 2022; 383: 132531.
[21] Ahmad R, Alqathama A, Aldholmi M, Riaz M, Eldin SM, Mahtab Alam M and Abdelmohsen SAM. Ultrasonic-assisted extraction of fenugreek flavonoids and its geographical-based comparative evaluation using green UHPLC-DAD analysis. Ultrason Sonochem 2023; 95: 106382.
[22] Wang W, Zhang X, Liu Q, Lin Y, Zhang Z and Li S. Study on extraction and antioxidant activity of flavonoids from hemerocallis fulva (daylily) leaves. Molecules 2022; 27: 2916.
[23] Wang Z, Li Z, Ye Y, Xie L and Li W. Oxidative stress and liver cancer: etiology and therapeutic targets. Oxid Med Cell Longev 2016; 2016: 7891574.
[24] Guo Z, Cheng J, Zheng L, Xu W and Xie Y. Mechanochemical-assisted extraction and hepatoprotective activity research of flavonoids from sea buckthorn (hippophaë rhamnoides L.) pomaces. Molecules 2021; 26: 7615.
[25] Wang Z, Wang W, Zhu C, Gao X and Chu W. Evaluation of antioxidative and neuroprotective activities of total flavonoids from sea buckthorn (hippophae rhamnoides L.). Front Nutr 2022; 9: 861097.
[26] Xia CX, Gao AX, Dong TT and Tsim KW. Flavonoids from seabuckthorn (hippophae rhamnoides L.) mimic neurotrophic functions in inducing neurite outgrowth in cultured neurons: signaling via PI3K/Akt and ERK pathways. Phytomedicine 2023; 115: 154832.
[27] Wang M, Zhang X, Zhang Z, Tong L, Yu S, Liu Y and Yang F. Flavonoid compounds in hippophae rhamnoides L. Protect endothelial cells from oxidative damage through the PI3K/Akt-eNOS pathway. Chem Biodivers 2024; 21: e202400300.
[28] Zhai T, Zhang X, Hei Z, Jin L, Han C, Ko AT, Yu X and Wang J. Isorhamnetin inhibits human gallbladder cancer cell proliferation and metastasis via PI3K/Akt signaling pathway inactivation. Front Pharmacol 2021; 12: 628621.
[29] Senggunprai L, Kukongviriyapan V, Prawan A and Kukongviriyapan U. Quercetin and EGCG exhibit chemopreventive effects in cholangiocarcinoma cells via suppression of JAK/STAT signaling pathway. Phytother Res 2014; 28: 841-848.
[30] Ma P, Li Z, Jin Y, Zuo J, Zhang Y, Dong A, Xiao D and Burenjargal M. Green and efficient extraction process of flavonoids from sea buckthorn fruits by natural deep eutectic solvents aided with ultrasound. Microchemical Journal 2024; 205: 111265.
[31] Baby J, Devan AR, Kumar AR, Gorantla JN, Nair B, Aishwarya TS and Nath LR. Cogent role of flavonoids as key orchestrators of chemoprevention of hepatocellular carcinoma: a review. J Food Biochem 2021; 45: e13761.

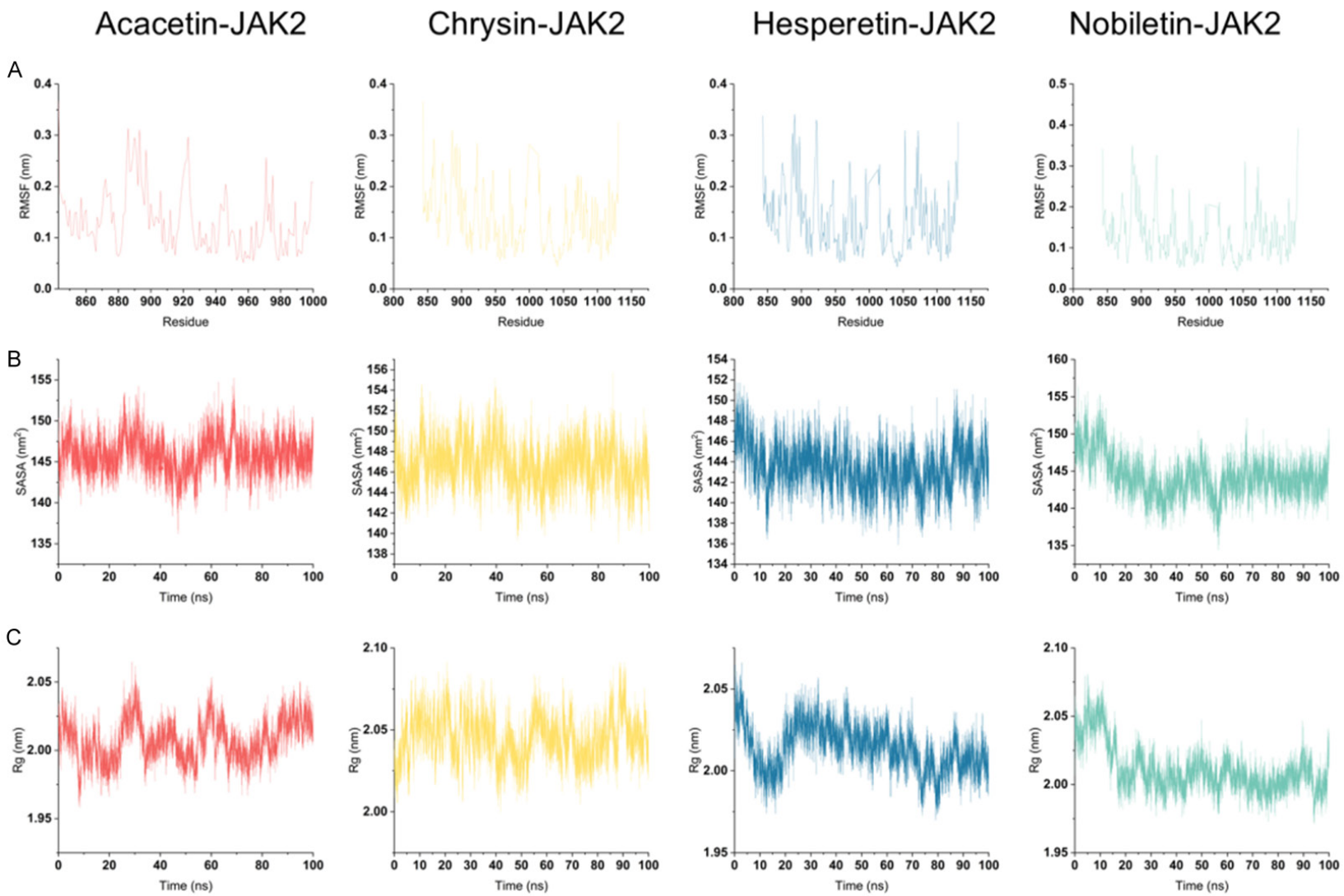

Figure S1. Comparative molecular dynamics analyses of flavonoid-JAK2 complexes. A. RMSF profiles with flexible regions marked for Hesperetin/Nobiletin. B. Solvent-accessible surface area (SASA) ranges reflecting dynamic interface adjustments. C. Radius of gyration (Rg) trajectories illustrating global structural compactness. Key differences in stabilization kinetics, flexibility, and solvent exposure are annotated.